Measurement and simulation of nuclear inelastic-scattering spectra of molecular crystals

H. Paulsen, H. Winkler, and A. X. Trautwein
Institut für Physik, Medizinische Universität Lübeck, D-23538 Lübeck, Germany

H. Grünsteudel*
European Synchrotron Radiation Facility, Boîte Postale 220, F-38043 Grenoble, France

V. Rusanov
Department of Atomic Physics, University of Sofia, BG-1126 Sofia, Bulgaria

H. Toftlund
Department of Chemistry, University of Odense, DK-5230 Odense, Denmark

(Received 24 July 1998)

A procedure is presented that allows us to simulate from first principles the normalized spectra of nuclear inelastic scattering (NIS) of synchrotron radiation by molecular crystals containing a Mössbauer isotope. Neglecting intermolecular vibrations the NIS spectrum is derived from the normal modes of the free molecule, that are calculated with the density-functional method B3LYP. At low temperatures the inelastic part of the calculated NIS spectrum is a superposition of peaks that correspond to the individual vibrational modes of the molecule. The area of each peak is proportional to that part of the mean-square displacement of the Mössbauer isotope that is due to the corresponding vibrational mode. Angular-dependent NIS spectra have been recorded for a guanidinium nitroprusside single crystal and temperature-dependent NIS spectra for the spin-crossover system $[Fe(tpa)(NCS)_2]$ [tpa=tris(2-pyridylmethyl)amine]. Qualitative agreement is achieved between measured and simulated spectra for different crystal orientations of guanidinium nitroprusside. A remarkable increase of the iron-ligand bond stretching upon spin crossover has unambiguously been identified by comparing the measured NIS spectra of $[Fe(tpa)(NCS)_2]$ with the theoretical simulations.
[S0163-1829(99)03102-1]

I. INTRODUCTION

The recently developed method of nuclear inelastic scattering (NIS) of synchrotron radiation,[1,2] which has become available as spectroscopic method with the third generation of synchrotron radiation sources, allows the investigation of the dynamics of a Mössbauer nucleus in solid state, liquids or gases. The information about the lattice dynamics obtained by conventional Mössbauer spectroscopy is summarized in a single parameter, the Lamb-Mössbauer factor f_{LM}, which gives the recoilless fraction of nuclear resonant absorption. NIS instead provides a complete energy spectrum of the absorption probability, which is recorded by detuning the energy of the incident synchrotron radiation with respect to the resonance of the Mössbauer nucleus. In solids this spectrum is determined by the vibrational density of states (VDOS), in liquid or gaseous samples by the normal modes of molecular vibration. Although part of the information gained with NIS can be obtained with other methods like neutron scattering, IR and Raman spectroscopy, NIS should be regarded as a complementary method, because it allows us to measure phonons also in the region $\gtrsim 50$ meV, and because it does focus on the partial VDOS of specific isotopes in a lattice or in a molecule, in the present case ^{57}Fe.

In solids the partial VDOS can directly be derived from the measured NIS spectra.[2,3] If, on the other hand, the partial VDOS, in the case of a cubic Bravais lattice, or, in the general case, the projected partial VDOS is known from experiment or theory, the corresponding NIS spectra can be simulated, as has been proved for α-iron and ferric borate.[4,5] This is, however, rather difficult for molecular crystals. For this reason an alternative procedure is presented here, where NIS spectra of molecular crystals are simulated from first principles using the calculated normal modes of the molecule *in vacuo*. The geometry and the vibrational modes of the molecule are calculated by applying the density-functional theory (DFT), which has been established as the most promising approach to the calculation of vibrational spectra of large molecules containing transition metals.[6] In a low-temperature approximation it is described how the individual molecular vibrations contribute to the NIS spectrum and to the mean-square displacement (msd) of the ^{57}Fe nucleus.

To test this simulation procedure and to illustrate some applications of NIS on molecular crystals, two different iron compounds, $(CN_3H_6)_2[Fe(CN)_5NO]$ (guanidinium nitroprusside) and $[Fe(tpa)(NCS)_2]$ (tpa=tris(2-pyridylmethyl)amine), are investigated. Both compounds are very promising materials for optical information storage with extremely high capacity.[7,8] Guanidinium nitroprusside (GNP) is used here as a calibration standard since nitroprusside complexes have been studied in detail in the past decades by a variety of experimental and theoretical methods. In addition GNP single crystals are very suitable to study the anisotropy of molecular vibrations because the two nonequivalent nitroprusside anions (Fig. 1) in the unit cell of GNP have almost the same orientation.[9] The

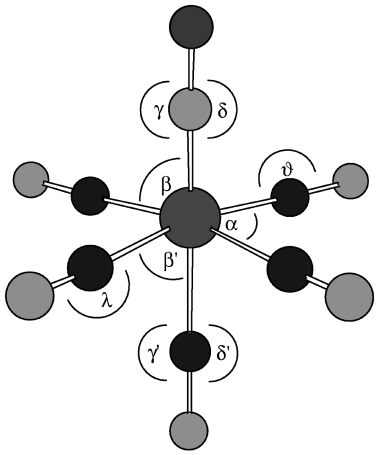

FIG. 1. Geometry of the $[Fe(CN)_5NO]^{2-}$ anion *in vacuo* optimized with B3LYP/6-311+G(2d,p). The small greek letters define intramolecular bending modes.

$[Fe(tpa)(NCS)_2]$ complex (Fig. 2) belongs to the family of thermally driven spin-crossover complexes, which exhibit a transition from a low-spin (LS) to a high-spin (HS) state by increasing the temperature. IR measurements on several spin-crossover complexes with a central $[FeN_6]$ octahedron indicate a remarkable increase of the Fe-N bond stretching frequencies from about 25 to 30 meV in the HS state to about 50 to 60 meV in the LS state.[10] In this case NIS turns out a very valuable alternative to IR and Raman spectroscopy because the Fe-N stretching modes can be definitely identified in the NIS spectra, whereas the IR and Raman spectra are rather complex in this frequency region[11] making an unambiguous assignment of these modes very difficult.

II. SIMULATION OF NIS SPECTRA

The nuclear resonant absorption of γ quanta has been used for the investigation of lattice dynamics since the discovery of the Mössbauer effect.[12] The bulk of these applications was restricted to the determination of the elastic (or recoilless) fraction f_{LM} of the integrated nuclear absorption probability density $S(E)$, where $E=E_\gamma-E_{\mathrm{res}}$ denotes the difference between the energy of the incident radiation E_γ and the nuclear resonance energy of ^{57}Fe, E_{res}. Only recently synchrotron radiation sources with sufficient intensity became available that allow us to vary the energy difference E in the range of phonons. If the incident radiation from the synchrotron is detuned with respect to E_{res}, nuclear absorption requires the simultaneous creation (for $E>0$) or annihilation (for $E<0$) of phonons.

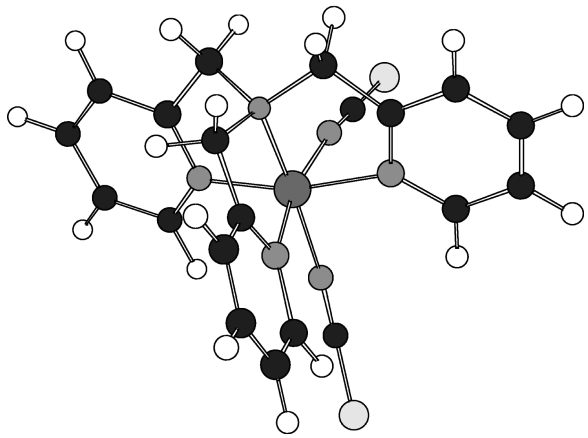

FIG. 2. Geometry of the HS isomer of $[Fe(tpa)(NCS)_2]$ optimized with B3LYP/3-21G*.

In an actual NIS experiment the energy difference E is varied in steps of ε, counting at each step the number of γ quanta that experience incoherent nuclear scattering. This scattering process involves excitation of the 14.413 keV nuclear resonance of ^{57}Fe (lifetime $\tau=141$ ns) followed by the emission of a γ quantum with the same energy ($\approx 8\%$ probability) or by the emission of a conversion electron and subsequent K-fluorescence radiation ($\approx 92\%$ probability). The time delay of the γ- or K-fluorescence radiation allows efficient discrimination of NIS from electronic scattering.

The number of delayed events that are counted for each energy step $E_n=n\varepsilon$ is denoted by I_n $(n=0,\pm 1,\pm 2,\ldots)$. For samples with finite thickness the increased attenuation of the incident radiation at the nuclear resonance[2] leads to a reduction of the count rate I_0 and to an overestimation of the absorption probability in the inelastic part of the spectrum. As a consequence the first moment $\overline{E}=(\Sigma_j E_j I_j)/(\Sigma_j I_j)$ of the energy can be distinctly larger than the average of the energy that is actually transferred to the lattice. According to Lipkin's sum rule[13] the average transferred energy equals the recoil energy $E_R=k^2\hbar^2/2m$ of the free ^{57}Fe nucleus; m is the nuclear mass and k is the length of the wavevector $\mathbf{k}$ of the incident synchrotron radiation. Lipkin's sum rule can be used to avoid the overestimation of the inelastic spectrum,[2] essentially by multiplying the measured spectrum with the factor $E_R/\overline{E}$. In the present study a modified procedure has been applied that allows to reconstruct also the elastic peak giving the corrected count rates

$$I_n'=I_n+\varepsilon R(E_n)\left(\frac{\overline{E}}{E_R}-1\right)\sum_j I_j. \tag{1}$$

The second term on the right side compensates for the increased attenuation of the incident beam at nuclear resonance. The resolution function $R(E)$, which describes the energy distribution of the incident radiation, is assumed to be an even function. From the corrected count rates I_n' the normalized absorption probability density $S(E_n)=I_n'/(\varepsilon\Sigma_j I_j')$ can be extracted.

In the solid state $S(E)$, or more generally the anisotropic absorption probability density $S(E,\hat{\mathbf{k}})$, can be simulated theoretically, if the projected partial VDOS, $g_{\mathrm{Fe}}(E,\hat{\mathbf{k}})$, is available, with $\hat{\mathbf{k}}=\mathbf{k}/k$. $S(E,\hat{\mathbf{k}})$ can be written as sum of the elastic part, that is due to the recoilless absorption, and of the inelastic part consisting of the multiphonon contributions $S_n(E,\hat{\mathbf{k}})$:

$$S(E,\hat{\mathbf{k}})=f_{\mathrm{LM}}(\hat{\mathbf{k}})\,\delta(E)+\sum_{n=1}^{\infty} S_n(E,\hat{\mathbf{k}}). \tag{2}$$

The anisotropic Lamb-Mössbauer factor $f_{\mathrm{LM}}(\hat{\mathbf{k}})$ is obtained from normalization of $S(E,\hat{\mathbf{k}})$. With the one-phonon contribution

$$S_1(E,\hat{\mathbf{k}}) = f_{\mathrm{LM}}(\hat{\mathbf{k}})\frac{E_R}{E}\frac{g_{\mathrm{Fe}}(|E|,\hat{\mathbf{k}})}{1-e^{-\beta E}} \tag{3}$$

($\beta = 1/k_B T$) all higher multiphonon contributions

$$S_n(E,\hat{\mathbf{k}}) = \frac{1}{n f_{\mathrm{LM}}(\hat{\mathbf{k}})}\int_{-\infty}^{+\infty} S_1(E',\hat{\mathbf{k}}) \times S_{n-1}(E-E',\hat{\mathbf{k}})dE' \quad (n \geqslant 2) \tag{4}$$

can be computed iteratively.[5]

This approach, however, is not suitable for liquids and gases, or, as in the present case, for molecular crystals. For this reason an alternative approach is described in the following, that can be used to simulate $S(E,\hat{\mathbf{k}})$ outside the energy range of *inter*molecular vibrations, i.e., for $E \gtrsim 15$ meV for the complexes discussed here. In this molecular approximation only the $L = 3N-6$ (N is the number of atoms) discrete *intra*molecular vibrations of the molecule *in vacuo* (in general corresponding to the L highest optical branches of the phonon spectrum of the molecular crystal) are considered whereas the *inter*molecular vibrations (corresponding to the three acoustical branches and, generally, to the lowest three optical branches) are disregarded, i.e., the center of mass and—in case of small amplitudes—the inertial tensor of the molecule are assumed to be fixed in space.

The probability density of nuclear absorption of a molecular complex containing only one ^{57}Fe nucleus is described by

$$S(E,\hat{\mathbf{k}}) = \sum_{i,f}\frac{e^{-\beta E_i}}{\mathcal{Z}}|\langle f|e^{-i\mathbf{k}\cdot\mathbf{u}}|i\rangle|^2\frac{\Gamma/2\pi}{(E_f-E_i-E)^2+\Gamma^2/4}, \tag{5}$$

where $\mathbf{u}$ stands for the displacement of the iron nucleus, E_i and E_f denote the energies of the initial and the final vibrational states of the molecular complex, $|i\rangle$ and $|f\rangle$, respectively, Γ is the linewidth of the vibrational transition, and $\mathcal{Z}$ is the partition function. To avoid the explicit summation over final states, the Lorentzian is Fourier transformed and the operator $\exp(-i\mathbf{k}\cdot\mathbf{u})$ is written in the interaction representation[14]

$$S(E,\hat{\mathbf{k}}) = \frac{1}{h}\int_{-\infty}^{+\infty}\langle e^{-i\mathbf{k}\cdot\mathbf{u}(0)}e^{+i\mathbf{k}\cdot\mathbf{u}(t)}\rangle e^{itE/\hbar-|t|\Gamma/2\hbar}dt. \tag{6}$$

The angular brackets $\langle \ldots \rangle$ represent both the quantum-mechanical and the thermal average. In the harmonic approximation the expectation value of the time-dependent operators can be replaced by the exponential of a displacement correlation function[15]

$$\langle \exp(-i\mathbf{k}\cdot\mathbf{u}(0))\exp(+i\mathbf{k}\cdot\mathbf{u}(t))\rangle = \exp\langle k^2[\hat{\mathbf{k}}\cdot\mathbf{u}(0)][\hat{\mathbf{k}}\cdot\mathbf{u}(t)]\rangle. \tag{7}$$

The exponent on the right side of the equation can be decomposed into a sum of L terms proportional to $\langle[\hat{\mathbf{k}}\cdot\mathbf{u}_l(0)][\hat{\mathbf{k}}\cdot\mathbf{u}_l(t)]\rangle$, which represent the contributions from the normal modes $l = 1,\ldots,L$. In the harmonic approximation these modes correspond to independent harmonic oscillators with reduced coordinates q_l and vibrational energies E_l. The reduced coordinates can be transformed into the Cartesian coordinates of the nuclei using the normalized eigenvectors $\mathbf{B}_l$ of the dynamical matrix. Only the projections of these $3N$-dimensional vectors into the three-dimensional subspace of the Cartesian iron coordinates, $\mathbf{b}_l$, are necessary for the determination of the displacement vector $\mathbf{u}$ of the iron nucleus, that can be written as a sum of L terms $\mathbf{u}_l = \mathbf{b}_l q_l/\sqrt{m}$. Using the known correlation function of the harmonic oscillator, the lth contribution to the displacement correlation of the iron nucleus can be written as

$$\langle[\hat{\mathbf{k}}\cdot\mathbf{u}_l(0)][\hat{\mathbf{k}}\cdot\mathbf{u}_l(t)]\rangle = \frac{(\hat{\mathbf{k}}\cdot\mathbf{b}_l)^2 E_R}{2k^2E_l\sinh(\beta E_l/2)} \times [e^{+\beta E_l/2-itE_l/\hbar}+e^{-\beta E_l/2+itE_l/\hbar}]. \tag{8}$$

With this expression the exponential on the right side of Eq. (7) can be expanded into the modified Bessel functions I_n of the first kind and nth order, and insertion of this expansion into Eq. (6) leads to

$$S(E,\hat{\mathbf{k}}) = \frac{e^{-\langle(\mathbf{k}\cdot\mathbf{u})^2\rangle}}{h}\int_{-\infty}^{+\infty}e^{itE/\hbar-|t|\Gamma/2\hbar} \times\prod_{l=1}^{L}\sum_{n_l=-\infty}^{+\infty}e^{\beta n_l E_l/2}I_{|n_l|}(C_l(\hat{\mathbf{k}}))e^{-itn_lE_l/\hbar}dt. \tag{9}$$

Here the symbols $C_l(\hat{\mathbf{k}})$ stand for

$$C_l(\hat{\mathbf{k}}) = \langle(\mathbf{k}\cdot\mathbf{u}_l)^2\rangle/\cosh(\beta E_l/2). \tag{10}$$

For the actual computation of the probability density as given in Eq. (9), only a special case of the displacement correlation function in Eq. (8) is needed, the projected msd contributions

$$\langle(\hat{\mathbf{k}}\cdot\mathbf{u}_l)^2\rangle = (\hat{\mathbf{k}}\cdot\mathbf{b}_l)^2(E_R/k^2E_l)\coth(\beta E_l/2), \tag{11}$$

and the total projected msd $\langle(\hat{\mathbf{k}}\cdot\mathbf{u})^2\rangle = \Sigma_{l=1}^{L}\langle(\hat{\mathbf{k}}\cdot\mathbf{u}_l)^2\rangle$. The term n_lE_l in Eq. (9) describes the net amount of energy that is transferred to the lth vibrational mode. If n_l is negative, the number of deexcitations exceeds the number of excitations. The infinite series on the right side of Eq. (9) is absolutely convergent and the product over l can be expanded into an L-fold sum. Solving the integral and reordering the terms in Eq. (9) the probability density takes its final form

$$S(E,\hat{\mathbf{k}}) = e^{-\langle(\mathbf{k}\cdot\mathbf{u})^2\rangle}\sum_{n_1=-\infty}^{+\infty}\sum_{n_2=-\infty}^{+\infty}\cdots\sum_{n_L=-\infty}^{+\infty}e^{\beta E_{\mathrm{vib}}/2} \times\frac{\Gamma/2\pi}{(E-E_{\mathrm{vib}})^2+\Gamma^2/4}\prod_{l=1}^{L}I_{|n_l|}(C_l(\hat{\mathbf{k}})), \tag{12}$$

that is used in the following to simulate the absorption probability density of the complexes under study. The energy $E_{\mathrm{vib}} = \Sigma_{l=1}^{L}n_lE_l$ represents the increase ($E_{\mathrm{vib}} > 0$) or decrease ($E_{\mathrm{vib}} < 0$) of the vibrational energy of the molecule. If the linewidth Γ of the vibrational transition is small in comparison to the energy resolution of the experimental setup, the

Lorentzian on the right side of Eq. (12) can be replaced by a δ function without loss of accuracy.

Assuming weak coupling between intra- and intermolecular vibrations, the anisotropic Lamb-Mössbauer factor $f_{\mathrm{LM}}(\hat{\mathbf{k}})$ can be factorized into a lattice factor $f_{\mathrm{lat}}(\hat{\mathbf{k}})$ and a molecular factor[16]

$$f_{\mathrm{mol}}(\hat{\mathbf{k}})=e^{-\langle(\mathbf{k}\cdot\mathbf{u})^2\rangle}\prod_{l=1}^{L} I_0(C_l(\hat{\mathbf{k}})). \tag{13}$$

The latter is obtained by integration of the elastic part of the nuclear absorption probability. For this elastic (''zero-phonon'') part only those terms in Eq. (12) apply, which correspond to zero excitation of all molecular vibrations or for which the number of excitations equals the number of deexcitations ($n_l=0$ for $l=1,\ldots,L$).

For the dominating ''one-phonon'' contribution to the inelastic part, which corresponds to a single excitation or deexcitation of one molecular vibration l', only those terms of the sum in Eq. (12) contribute where in the product of the $I_{|n_l|}$ all n_l are zero except for one, i.e., $n_{l'}$, which must be $+1$ or -1. For $\beta E_l \gg 1$ the modified Bessel functions can be replaced by $I_0(C_l(\hat{\mathbf{k}}))\sim 1$ and $I_1(C_l(\hat{\mathbf{k}}))\sim C_l(\hat{\mathbf{k}})/2$ leading to the low-temperature approximation

$$S_1(E,\hat{\mathbf{k}})\sim f_{\mathrm{mol}}(\hat{\mathbf{k}})\frac{E_R}{E}\sum_{l=1}^{L}\delta(E_l-E)(\hat{\mathbf{k}}\cdot\mathbf{b}_l)^2. \tag{14}$$

This equation is the molecular equivalent to the one-phonon contribution in solid state [Eq. (3)]. The sum on the right side of Eq. (14) corresponds to the projected partial VDOS, $g_{\mathrm{Fe}}(E,\hat{\mathbf{k}})$, in a single crystal. At low temperatures the probability for the deexcitation of a molecular vibration or for the simultaneous excitation of more than one vibration vanishes. Using Eq. (11) the absorption probability density can then be written as a superposition of the elastic part and of L contributions to the inelastic part:

$$S(E,\hat{\mathbf{k}})\sim e^{-\langle(\mathbf{k}\cdot\mathbf{u})^2\rangle}\left[\delta(E)+k^2\sum_{l=1}^{L}\delta(E-E_l)\langle(\hat{\mathbf{k}}\cdot\mathbf{u}_l)^2\rangle\right]. \tag{15}$$

Each of the L contributions of the inelastic part is proportional to the projected msd $\langle(\hat{\mathbf{k}}\cdot\mathbf{u}_l)^2\rangle$ of the corresponding vibrational mode.

Prior to the simulation of $S(E,\hat{\mathbf{k}})$, DFT calculations have to be performed, to yield the vibrational energies E_l and the projected eigenvectors $\mathbf{b}_l$ of the dynamical matrix, which comprise all the necessary information of the specific molecule.

III. MATERIALS AND METHODS

A. Computational details

DFT calculations were performed for the nitroprusside anion *in vacuo* and for the HS and LS isomers of $[\mathrm{Fe(tpa)(NCS)_2}]$ using the B3LYP method,[17] implemented in the GAUSSIAN94 program system[18] together with the split valence 3-21G* basis set.[19] For the nitroprusside anion additional calculations were performed with the 6-311 $+$G($2d,p$) basis set[20] for C, N, and O together with the Wachters-Hay basis set[21] for Fe. The geometries were fully optimized applying the Berny algorithm to redundant internal coordinates.[22] Force constants were calculated analytically at the same level of theory using the optimized geometries, and the resulting vibrational frequencies were corrected by the scaling factor 0.9613 as has been proposed by Wong[23] for the 6-31G* basis set. To obtain the projected eigenvectors $\mathbf{b}_l$, the iron components of the normal coordinate vectors provided by the GAUSSIAN94 program had to be multiplied by the factor $\sqrt{m/m_l}$, where m_l is the reduced mass of the lth normal mode.

The probability density $S(E,\hat{\mathbf{k}})$ was calculated according to Eq. (12) and folded with the resolution function $R(E)$, which represents the energy distribution of the incident radiation. In the present case $R(E)$ is a normalized Gaussian with 6 meV full linewidth. For the polycrystalline $[\mathrm{Fe(tpa)(NCS)_2}]$ sample $S(E)$ was calculated by numerical integration of $S(E,\hat{\mathbf{k}})$ over $\hat{\mathbf{k}}$.

B. Samples

GNP single crystals with a size of $10\times10\times50$ mm^3 were grown from an aqueous solution of $(\mathrm{CN_3H_6})_2[\mathrm{Fe(CN)_5NO}]$ by slow evaporation of the solvent at about 310 K. The conditions of the crystal growth, as well as all chemical and structural features of GNP are discussed in detail in Ref. 9. For NIS and IR measurements single crystals of different thickness varying from 50 to 2500 μm have been used. The samples were cut from larger crystals of high quality with the surface normal in the crystallographic **a** and **c** directions (**a**-cut and **c**-cut, respectively). The thinnest crystals that could be produced by mechanical polishing had a thickness of 150 μm. Even thinner samples were prepared by etching these crystals in a 3:1 mixture of distilled water and *n*-propanol until a thickness of about 50 μm was reached. Lower thickness led to mechanical destruction of the crystals. The preparation of the polycrystalline sample of $[\mathrm{Fe(tpa)(NCS)_2}]$ is described in Ref. 24.

C. Nuclear inelastic scattering

NIS spectra were recorded at the Nuclear Resonance Beamline ID 18 of the European Synchrotron Radiation Facility (ESRF) in Grenoble, France.[25] The 6 GeV electron storage ring was operated in single bunch mode for GNP and in a 16 bunch mode for $[\mathrm{Fe(tpa)(NCS)_2}]$. The purity of the filling (population of parasitic bunches compared to the single bunch) was better than 10^{-9}. The incident beam was monochromatized by a double-crystal Si(111) premonochromator to the bandwidth of 2.5 eV at the energy of 14.413 keV. A further decrease of bandwidth down to 6 meV was obtained with a ''nested'' high-resolution monochromator.[26] This beam was used to excite the 14.413 keV nuclear level of ^{57}Fe in a sample mounted in a closed-cycle cryostat to allow measurements at different temperatures. An avalanche photodiode with 10×10 mm^2 area, 100 μm active thickness, and a time resolution of less than 1 ns has been used as a detector[27] to count the 14.413 keV γ quanta and, mainly, the K-fluorescence photons ($\approx$6.4 keV). The data were

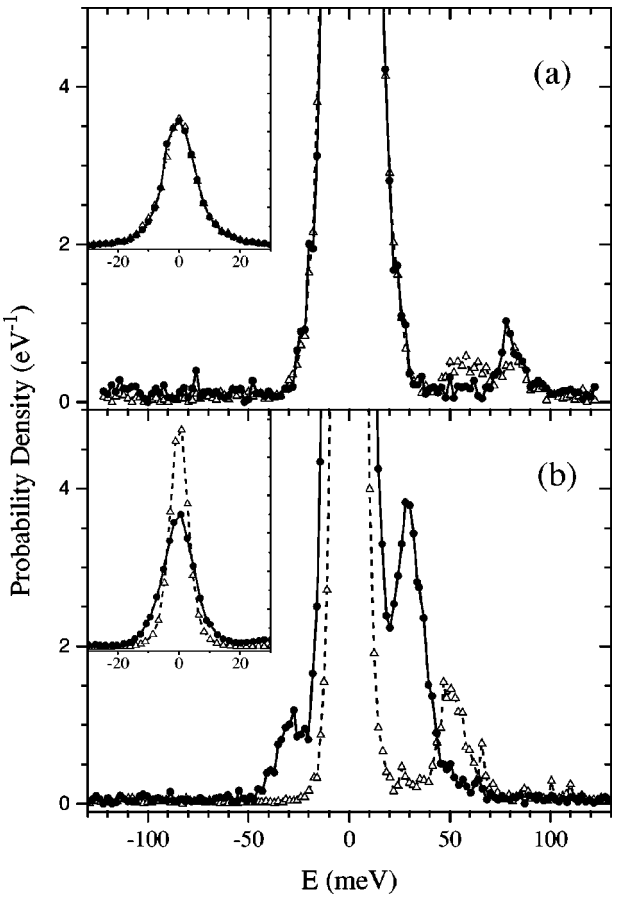

FIG. 3. Measured NIS spectra of (a) the **a**-cut (△) and **c**-cut (●) crystals of GNP, and (b) of the HS (●) and LS (△) isomers of $[Fe(tpa)(NCS)_2]$. The solid and dashed lines serve as a guide to the eyes.

collected during several energy scans with 140 steps on average, each with 2 meV step size and 10 s measuring time. All individual scans were corrected for the approximately 9% decrease of beam intensity of the storage ring during the 1500 s required for each scan and added up afterwards.

D. Infrared spectroscopy

Infrared spectra for GNP were recorded with a BOMEM DA3 Fourier spectrometer with 0.6 meV resolution, a beamsplitter of KBr, and a pyroelectric detector DTGS/KBr using single crystals of about 150 μm thickness. However, in the spectral interval between 50 and 125 meV where the absorption is very strong even thinner crystal cuts of 50 μm thickness were needed. In addition infrared spectra were taken from guanidinium hydrochloride CN_3H_5ClH, which is one of the chemical components used for the synthesis of the guanidinium nitroprusside.

IV. EXPERIMENTAL RESULTS

A. Nuclear inelastic scattering

NIS spectra have been recorded for the **a**-cut and **c**-cut crystals of GNP at room temperature and for a polycrystalline sample of $[Fe(tpa)(NCS)_2]$ at 34 K (LS state) and at 200 K (HS state). The NIS spectra of the **a**-cut and **c**-cut crystals of GNP are shown in Fig. 3(a). They exhibit central peaks of 11 meV linewidth (full width at half maximum), which is almost twice as large as the energy resolution of the incident radiation and indicates that a considerable part of the central peak belongs to the inelastic part of the spectrum. Apart from the central peak, nonvanishing probability density is observed in the range between 50 and 90 meV. In this range the measured probability density of the **a**-cut crystal is significantly different from that of the **c**-cut crystal. The NIS spectra of the HS and LS isomers of $[Fe(tpa)(NCS)_2]$ [Fig. 3 (b)] exhibit central peaks of 12 and 7 meV linewidth, respectively, and a pronounced inelastic peak at 30 meV in the HS state and at 50 meV in the LS state. Comparing the intensity of the pronounced inelastic peaks in the HS and the LS spectrum it should be kept in mind, that the HS peak at 30 meV is located on the shoulder of the corresponding central peak. The linewidth of the LS peak observed at 50 meV is significantly larger than the linewidth of the corresponding central peak. The LS peak should, therefore, be regarded as a superposition of two or more individual peaks. The LS spectrum exhibits another, rather small peak at 66 meV (see also Fig. 5), which is invisible in the HS spectrum. In the negative energy domain ($E_\gamma < E_{\rm res}$) the probability density vanishes at 34 K (LS), whereas a small peak at -30 meV can be observed at 200 K (HS).

The first moments of the NIS spectra of GNP and of the NIS spectrum of the HS isomer of $[Fe(tpa)(NCS)_2]$ (1.8 to 2.0 meV) are in reasonable agreement with the recoil energy $E_R = 1.96$ meV of the free ^{57}Fe nucleus, as expected according to Lipkin's rule, whereas the first moment of the NIS spectrum of the LS isomer of $[Fe(tpa)(NCS)_2]$ amounts to 4 meV, which is about twice as large as E_R. For the two complexes under study a correlation between the first moment of the NIS spectrum and the Lamb-Mössbauer factor $f_{\rm LM}$ is found. In those cases where the first moment is close to E_R, the Lamb-Mössbauer factor is small [$f_{\rm LM}(\mathbf{a}) = 0.12(1)$ and $f_{\rm LM}(\mathbf{c}) = 0.20(1)$ for the respective crystals of GNP, and $f_{\rm LM}^{\rm HS} = 0.21(1)$ for the HS isomer of $[Fe(tpa)(NCS)_2]$], whereas a large Lamb-Mössbauer factor has been measured for the LS isomer of $[Fe(tpa)(NCS)_2]$ [$f_{\rm LM}^{\rm LS} = 0.68(1)$],[28] for which the first moment of the NIS spectrum significantly exceeds the recoil energy E_R. The increased attenuation of the incident radiation at nuclear resonance can be neglected if $f_{\rm LM}$ is small. For this reason only the NIS spectrum of the LS isomer of $[Fe(tpa)(NCS)_2]$ had to be corrected according to Eq. (1).

B. Infrared measurements

The IR spectra recorded with the **a**-cut and **c**-cut crystals of GNP exhibit three very strong absorption bands centered at 125, 205, and 410 meV, which represent vibrational modes of guanidinium as suggested by a separate IR measurement with guanidinium hydrochloride only (not shown). In the region from 260 to 310 meV, that is attributed to vibrational modes of the nitroprusside anion, a narrow absorption band with fine structure centered at about 267 meV is observed in the spectra for both crystal orientations.

In the IR spectra of very thin crystal cuts (50 μm) a number of strong, discrete lines are identified at 56, 60, 63, 70, 76, and 81 meV [Fig. 4(a)]. Comparison of the vibrational frequencies of the nitroprusside anion in GNP, as pre-

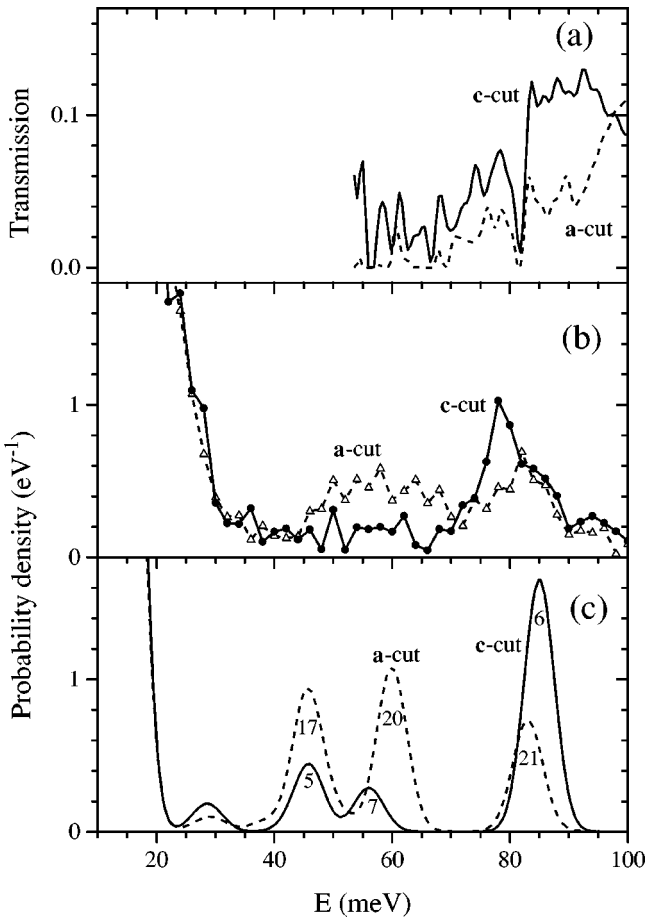

FIG. 4. IR spectra (a), and NIS spectra—measured (b) and simulated (c)—of the **a**-cut (dashed lines, △) and **c**-cut (solid lines, ●) crystals of GNP. The IR spectra were normalized to the same crystal thickness. The inelastic peaks in the simulated NIS spectra (c) are labelled according to the mode numbering in Table II.

sented here, with the corresponding results for sodium nitroprusside (SNP), taken from former studies,[29,30] does not provide any evidence for drastic frequency changes by going from GNP to SNP. However, the presence of the guanidinium cations complicates an unambiguous frequency assignment in GNP in comparison to some other nitroprussides.

V. COMPUTATIONAL RESULTS AND DISCUSSION

A. Guanidinium nitroprusside

The B3LYP method combined with two different basis sets has been used to calculate the geometry of the nitroprusside anion *in vacuo*, which has been restricted to C_{4v} symmetry. The deviations from 1 to 3 pm between the calculated bond lengths and the measured values for SNP (Table I) are very likely due to the neglected interactions between the nitroprusside anion and its counter-cations. Similar deviations are observed comparing nitroprussides with different cations, e.g., SNP,[31] barium nitroprusside and GNP.[9] The symmetry constraint is expected to have minor effect on the optimized geometry. Deviations from C_{4v} symmetry by 2 to 5° for the Fe-N-O bond angle and by less than 1 pm for the different bond lengths have been observed by x-ray studies on solid

TABLE I. Bond lengths in pm for the nitroprusside anion taken from x-ray measurements on GNP (Ref. 9) and from present calculations with the B3LYP method and two different basis sets.

	X ray	3-21G*	6-311+G(2*d*,*p*)
Fe-N	165	160	163
Fe-C_{ax}	195	195	197
Fe-C_{eq}	194	193	197
N-O	113	120	115
C_{ax}-N	115	117	116
C_{eq}-N	114	117	116

nitroprussides.[9,31] Therefore these deviations can be regarded as an upper bound for the deviations from C_{4v} symmetry in the free nitroprusside anion.

The 33 normal modes of the nitroprusside anion can be classified according to the five irreducible representations of the C_{4v} point group. The displacement of the iron nucleus is varying with the normal coordinates of the A_1 and E modes, while it remains zero for the other modes; therefore only the A_1 and E modes can be observed in the NIS spectra of GNP. Since the symmetry axes of the two nonequivalent nitroprussides anions in the unit cell of GNP approximately ($\pm 9°$) coincide with the crystallographic **c** axis, the A_1 modes, which are connected with the mean-square displacement (msd) of the iron nucleus parallel to the symmetry axis ($\mathbf{b}_l \| \mathbf{c}$), can only be observed in the **c**-cut NIS spectrum, whereas one out of each of the twofold degenerate E modes, which contribute to the msd of the iron nucleus perpendicular to the symmetry axis ($\mathbf{b}_l \perp \mathbf{c}$), is visible in the **a**-cut NIS spectrum.

The calculated normal modes are characterized in terms of bond stretching (s) and bending (α, β, β', γ, γ', λ, ϑ, see Fig. 1) vibrations (Table II). The carbon atom that is located on the symmetry axis is labeled with C_{ax}, the remaining four carbon atoms, lying in an equatorial plane, are labeled with C_{eq}. These assignments are in agreement with previous assignments, that result from a normal-coordinate analysis in valence force-field approximation.[30] According to their energy the vibrational modes can be divided into three groups: (i) six C-N or N-O bond stretching modes in the spectral range above 220 meV, (ii) six Fe-C or Fe-N stretching modes and 12 Fe-C-N or Fe-N-O bending modes (γ, γ', λ, ϑ) in the range from 35 to 90 meV, and (iii) nine C-Fe-C or C-Fe-N bending modes (α, β, β') in the range below 20 meV. Comparison of the vibrational frequencies calculated with the 6-311+G(2*d*,*p*) basis with the corresponding experimental frequencies obtained from IR and Raman measurements on SNP (Ref. 30) reveals deviations in the range from 1 to 5 % for the C-N and N-O stretching modes as well as for the Fe-N stretching and the Fe-N-O bending modes. Good agreement between measured and calculated frequencies is also achieved for the Fe-C-N bending modes (1 to 8%) whereas the calculated Fe-C stretching frequencies are between 12 and 19 % smaller than the measured frequencies for SNP. Comparable results from calculations with other nonlocal DF methods for the free nitroprusside anion and for solid NNP are reported in Refs. 7,32.

The vibrational frequencies calculated with the 3-21G* basis set differ from those calculated with the 6-311+G

TABLE II. Vibrational energies E_l, measured for SNP by IR and Raman spectroscopy and calculated for the free nitroprusside anion with B3LYP/6-311+G($2d,p$), and calculated contributions to the projected iron msd $\langle(\hat{\mathbf{k}}\cdot\mathbf{u}_l)^2\rangle$. (With $\hat{\mathbf{k}}=\mathbf{c}$ for A_1 modes and $\hat{\mathbf{k}}=\mathbf{a}$ for E modes.)

l [a]	Sym. spec.	Primary contribution[b]	E_l in meV		$\langle(\hat{\mathbf{k}}\cdot\mathbf{u}_l)^2\rangle$
			Exp. (Ref. 30)	Calc.	in pm^2
1	A_1	C_{ax}-N s	269.9	266.1	0.00
2		C_{eq}-N s	268.8	265.2	0.00
3		N-O s	241.4	228.9	0.00
4		Fe-C_{eq} s	51.2	41.7	0.01
5		Fe-C_{ax} s	52.1	45.9	0.23
6		Fe-N s	81.5	84.8	0.75
7		Fe-C-N ϑ	57.4	55.9	0.14
8		C-Fe-C,N β,β'	12.6	14.3	5.02
9	A_2	Fe-C-N λ		38.2	
10	B_1	C-N_{eq} s	268.3	264.6	
11		Fe-C_{eq} s	50.0	40.7	
12		Fe-C-N ϑ	49.2	50.6	
13		C,N-Fe-C β,β'	13.0	9.4	
14	B_2	Fe-C-N λ	52.8	53.7	
15		C-Fe-C α	11.4	13.0	
16	E	C-N_{eq} s	266.3	264.1	0.00
17		Fe-C_{eq} s	56.3	45.5	0.50
18		Fe-C-N ϑ	39.7	38.3	0.04
19		Fe-C-N λ	53.9	51.0	0.05
20		Fe-C-N γ'	62.1	59.9	0.54
21		Fe-N-O γ	82.7	83.0	0.35
22		C,N-Fe-C β,β'	8.8	7.7	1.99
23		C-Fe-C β,β'	18.9	14.5	3.74
24		C,N-Fe-C β,β'	12.3	12.3	1.10

[a]For comparison mode numbering has been adjusted to the convention used in Refs. 30.

[b]Assignment based on DFT calculations. s denotes stretching modes and small greek letters denote the bending modes defined in Fig. 1.

($2d,p$) basis set by less than 13%, for most modes by less than 5%. Hence, if only a modest precision is demanded and if the investigated molecules are quite large, the smaller but much less time-consuming basis set 3-21G* is an acceptable compromise.

The strongest molecular contributions to the projected iron msd [Eq. (11)] and to the nuclear absorption probability originate from the C-Fe-C and N-Fe-C bending modes (Table II). For these modes direct comparison between the measured and the calculated probability density is difficult because of the expected strong interactions between *intra*- and *inter*molecular vibrations. However, it should be noted that agreement of the measured and calculated energy range of these modes (8–19 meV) is obtained. Out of the 18 Fe-N,C stretching and Fe-C-N and Fe-N-O bending modes three A_1 modes and three E modes contribute significantly to the absorption probability. Two of these modes, the Fe-N stretching mode ($6A_1$) and the Fe-N-O γ bending mode ($21E$), give rise to prominent peaks in the **c**-cut and the **a**-cut spectrum, respectively, whereas the other four modes give rise to peaks that are too broad to be resolved in the experimental NIS spectra.

The linewidth of the measured peaks is significantly larger than the linewidth of the simulated peaks. Nevertheless qualitative agreement between the experimental and the simulated NIS intensity relations of the **a**-cut and **c**-cut spectra is obtained: in the spectrum of the **a**-cut crystal contributions to the absorption probability of similar size arise from modes $17E$, $20E$, and $21E$, whereas in the **c**-cut spectrum the contribution of mode A_1 is dominant in comparison to the contributions of modes $5A_1$ and $7A_1$ [Fig. 4(b) and 4(c), Table II].

The anisotropy of the nuclear absorption probability is closely related to the anisotropy of the iron msd. For the **a**-cut and **c**-cut crystals of GNP the molecular part of the iron msd along the crystallographic axes can be approximated by the sum of the msd contributions of the A_1 modes (**a**-axis) and E modes (**c**-axis), respectively, which are given in Table II.

The calculated iron msd along the **a**-axis (8 pm^2) is about 30% larger than the msd along the **c**-axis (6 pm^2) and correspondingly the calculated molecular Lamb-Mössbauer factor for the **a**-cut crystal [$f_{\mathrm{mol}}(\mathbf{a})=0.87$] is slightly smaller than the molecular Lamb-Mössbauer factor of the **c**-cut crystal [$f_{\mathrm{mol}}(\mathbf{c})=0.90$]. Comparison with the experimental Lamb-Mössbauer factors,[28] $f_{\mathrm{LM}}(\mathbf{a})=0.12(1)$ and $f_{\mathrm{LM}}(\mathbf{c})=0.20(1)$, indicates, that the by far largest part of the iron

msd must be due to intermolecular vibrations of the nitroprusside anions and its counter-cations.

B. $[Fe(tpa)(NCS)_2]$

For reasons of size the geometry optimization and the frequency calculation for $[Fe(tpa)(NCS)_2]$, containing 47 atoms with 292 electrons, have been performed with the 3-21G* basis set only. No x-ray structures are available that can be compared with the calculated geometries of $[Fe(tpa)(NCS)_2]$, but the calculated bond lengths of the HS and LS isomers qualitatively resemble the increase of the Fe-N bond distances upon spin crossover of about 10 to 20 pm observed in various spin-crossover complexes with a central $[FeN_6]$ octahedron.[10]

The vibrational spectra of the HS and the LS isomers of $[Fe(tpa)(NCS)_2]$ consist of 135 normal modes and are, in the following discussion, subdivided into a high-frequency region above 75 meV (which can be disregarded here, because the modes in this frequency range do practically not contribute to the iron msd) and a low-frequency region below 75 meV.

Among the 41 normal modes of the low-frequency region the iron-ligand bond stretching vibrations are of special interest here. In view of the results obtained for GNP, an error margin of about 10 to 20 % is estimated for the calculated Fe-N stretching frequencies, which can be considered as small in comparison to the expected drastic increase of these frequencies upon spin crossover. Due to the almost octahedral environment of the iron center three out of six Fe-N stretching modes are invisible in NIS and IR spectra. Those modes that transform according to the A_1 and E_g representations of the ideal octahedron do not contribute to the msd of the iron nucleus or to the variation of the electric dipole moment. Only the remaining three modes, that transform according to the T_{1u} representations can be observed in NIS and IR spectra. These three modes, with calculated frequencies of 29.9, 30.1, and 35.3 meV for the HS state and 42.8, 46.6, and 52.6 meV for the LS state, give rise to a prominent peak in the simulated NIS spectra of both isomers of $[Fe(tpa)(NCS)_2]$.

By IR spectroscopy[24] Fe-N bond stretching frequencies of 59.5 and 66.0 meV have been found for the LS isomer, while for the region below 35 meV, that is difficult to reach experimentally, no frequencies are reported. The Fe-N bond stretching frequencies calculated for the LS isomer are about 12.4 meV smaller than the IR values given above; however, they are in good agreement with the frequencies obtained from NIS. The broad peak at 50 meV observed in the measured NIS spectrum of the LS isomer (Fig. 5) represents the envelope of the three Fe-N stretching modes in the range of 45 to 55 meV. The pronounced peak at 30 meV in the NIS spectrum of the HS isomer is assigned to the same modes (Fig. 5). These modes reflect, according to the intensity of the peaks, the substantial contributions to the msd of the iron nucleus that is associated with the three T_{1u} Fe-N stretching modes.

According to the normal mode analysis the low-intensity peak at 66 meV in the measured NIS spectrum as well as the line at 65.7 meV in the IR spectrum must be assigned to a mode which has predominantly N-C-S bending character and

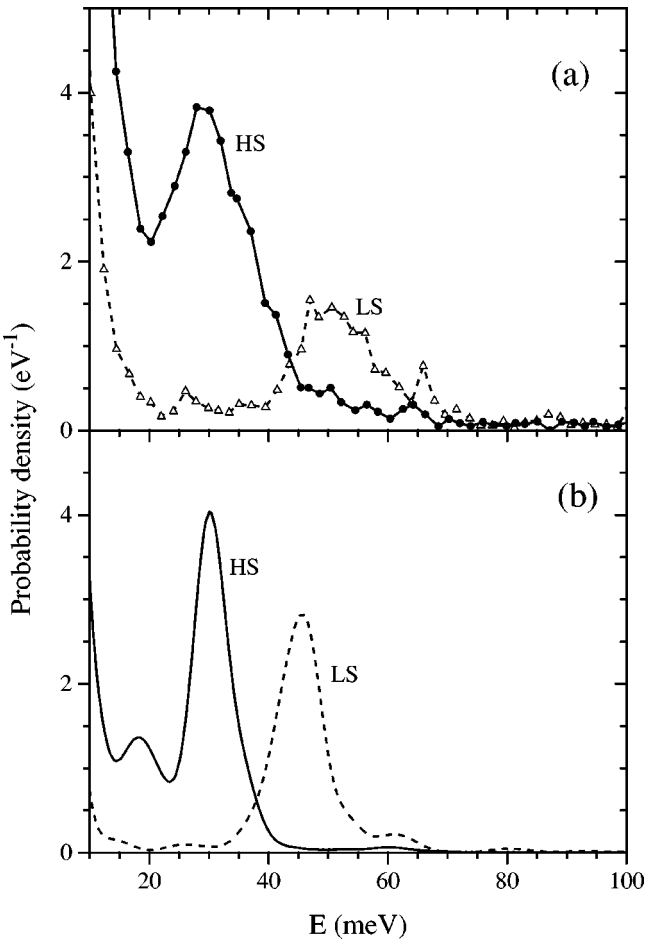

FIG. 5. Measured (a) and simulated (b) NIS spectra of the HS (solid lines, ●) and LS (dashed lines, △) isomers of $[Fe(tpa)(NCS)_2]$.

to some extent Fe-N stretching character. The mixed character of this mode is due to interactions between Fe-N stretching and N-C-S bending modes, which are close in energy in the LS isomer.

The calculated N-C-S bending modes of the HS isomer do not show any admixture of Fe-N stretching modes because of the relatively large energy gap of about 30 meV between these modes. Correspondingly the NIS spectrum of the HS isomer does not exhibit a peak at the respective energy. In summary, the NIS spectra of the LS isomer as well as the DFT calculations suggest, that the IR line attributed previously to an Fe-N bond stretching mode of the LS isomer should be assigned to a bending mode of the NCS group instead. As a result the frequency shift of the Fe-N stretching mode upon spin crossover is about 40% smaller than assumed earlier. DFT calculations for another spin-crossover complex with NCS groups, i.e., $[Fe(phen)_2(NCS)_2]$ (phen =1,10-phenanthroline), lead to a similar conclusion.

The measured Lamb-Mössbauer factor of $[Fe(tpa)(NCS)_2]$ is decreasing from $f_{LM}^{LS}=0.68(1)$ for the LS state at 34 K to $f_{LM}^{HS}=0.21(1)$ for the HS state at 200 K.[28] Comparison of these values with the calculated molecular Lamb-Mössbauer factors ($f_{mol}^{LS}=0.92$ and $f_{mol}^{HS}=0.52$) indicates, that for both spin states the major part of the iron msd is due to *inter*molecular vibrations. However, the msd of the

HS state contains, according to the calculations, also significant contributions from *intra*molecular vibrations.

VI. CONCLUSION

The energy spectra of nuclear inelastic scattering of synchrotron radiation by molecular crystals have been simulated in a molecular approximation using a normal mode analysis that was obtained from DFT calculations. The peaks observed in the inelastic part of the absorption spectrum can be related to individual molecular vibrational modes, where the position of the peak is given by the vibrational energy and the intensity of the peak is proportional to the contribution to the msd of the Mössbauer nucleus of the respective mode. From the sum of the molecular msd contributions a molecular Lamb-Mössbauer factor can be calculated, that means, the rigidity of the molecular crystal can be separated into a part that is due to interatomic forces within the molecule, and a part that is due to forces between the individual molecules of the crystal. NIS experiments with single crystals provide information about the anisotropy of the dynamics of the Mössbauer nucleus and about the anisotropy of the inter- and intramolecular forces, as has been demonstrated for GNP.

In the approach presented here the interactions between inter- and intramolecular vibrations have been neglected. However, NIS can be used to investigate these interactions, if the energy resolution of the incident radiation is reduced to the order of μeV by nuclear resonant filtering.

Due to its ability to focus on few modes out of a rather complex vibrational spectrum NIS can be a complementary or, for certain problems, even a superior alternative to conventional methods like IR and Raman spectroscopy. A good example is the investigation of iron(II) spin-crossover complexes as presented here. IR and Raman spectra are rather complex in the frequency range of the Fe-N bond stretching modes (20–60 meV). Even if the isotope technique is used the assignment of these modes to the observed bands often remains doubtful as has been demonstrated for $[Fe(tpa)(NCS)_2]$. In the NIS spectra, however, the Fe-N stretching modes could be unambiguously identified.

ACKNOWLEDGMENTS

The authors acknowledge the support by A. I. Chumakov, R. Rüffer, and H. F. Grünsteudel and by the relevant ESRF services during these measurements, and the financial support by the European Union (ERB-FMRX-CT-0199) via the TMR-TOSS-network, by the German Research Foundation (DFG) and by the German Federal Ministery for Education, Science, Research and Technology (BMBF). V.R. is very much indebted to the German Volkswagen-Foundation and to the Alexander von Humboldt-Foundation.

*On leave from the Department of Chemistry, University of Odense, Odense, Denmark.

[1] M. Seto, Y. Yoda, S. Kikuta, X. W. Zhang, and M. Ando, Phys. Rev. Lett. **74**, 3828 (1995).

[2] W. Sturhahn, T. S. Toellner, E. E. Alp, X. Zhang, M. Ando, Y. Yoda, S. Kikuta, M. Seto, C.W. Kimball, and B. Dabrowski, Phys. Rev. Lett. **74**, 3832 (1995).

[3] B. Fultz, T. A. Stephens, W. Sturhahn, T. S. Toellner, and E. E. Alp, Phys. Rev. Lett. **80**, 3304 (1998).

[4] A. I. Chumakov, R. Rüffer, A. Q. R. Baron, H. Grünsteudel, and H. F. Grünsteudel, Phys. Rev. B **54**, 9596 (1996).

[5] A. I. Chumakov, R. Rüffer, A. Q. R. Baron, H. Grünsteudel, H. F. Grünsteudel, and V. G. Kohn, Phys. Rev. B **56**, 10 758 (1997).

[6] N. Rösch and H. Jörg, J. Chem. Phys. **84**, 5967 (1986); J. Andzelm and E. Wimmer, *ibid.* **96**, 1280 (1992); B. Delley, M. Wrinn, and H. P. Lüthi, *ibid.* **100**, 5785 (1994); V. Jonas and W. Thiel, *ibid.* **105**, 3636 (1996); C. Sosa, J. Andzelm, B. C. Elkin, E. Wimmer, K. D. Dobbs, and D. A. Dixon, J. Phys. Chem. **96**, 6630 (1992); R. Fournier and I. Papai, in *Recent Advances in Density Functional Methods*, edited by D. P. Chong (World Scientific, 1996), Part I; A. Berces and T. Ziegler, *Topics in Current Chemistry* (Springer, Berlin, 1996), Vol. 182, p. 41.

[7] B. Delley, J. Schefer, and Th. Woike, J. Chem. Phys. **107**, 10 067 (1997).

[8] P. Gütlich, A. Hauser, and H. Spiering, Angew. Chem. **106**, 2109 (1994).

[9] C. Retzlaff, W. Krumbe, M. Dörffel, and S. Haussühl, Z. Kristallogr. **189**, 141 (1989).

[10] E. König, Struct. Bonding (Berlin) **76**, 51 (1991).

[11] J. H. Takemoto and B. Hutchinson, Inorg. Chem. **12**, 705 (1973).

[12] R. L. Mössbauer, Z. Phys. **151**, 124 (1958).

[13] H. J. Lipkin, Ann. Phys. (Paris) **9**, 332 (1960).

[14] K. S. Singwi and A. Sjölander, Phys. Rev. **120**, 1093 (1960).

[15] A. A. Maradudin, Solid State Phys. : *Advances in Research and Applications* (Academic, New York, 1966), Vol. 18, p. 274.

[16] J. Jung, H. Spiering, Z. Yu, and P. Gütlich, Hyperfine Interact. **95**, 107 (1995).

[17] A. D. Becke, J. Chem. Phys. **98**, 5648 (1993); C. Lee, W. Yang, and R. G. Parr, Phys. Rev. B **37**, 785 (1988).

[18] M. J. Frisch *et al.*, GAUSSIAN 94, Revision C.3, Gaussian, Inc., Pittsburgh, PA, 1995.

[19] J. S. Binkley, J. A. Pople, and W. J. Hehre, J. Am. Chem. Soc. **102**, 939 (1980); M. S. Gordon, J. S. Binkley, J. A. Pople, W. J. Pietro, and W. J. Hehre, *ibid.* **104**, 2797 (1982): W. J. Pietro, M. M. Francl, W. J. Hehre, D. J. Defrees, J. A. Pople, and J. S. Binkley, *ibid.* **104**, 5039 (1982).

[20] R. Ditchfield, W. J. Hehre, and J. A. Pople, J. Chem. Phys. **54**, 724 (1971); W. J. Hehre, R. Ditchfield, and J. A. Pople, *ibid.* **56**, 2257 (1972); P. C. Hariharan and J. A. Pople, Mol. Phys. **27**, 209 (1974); M. S. Gordon, Chem. Phys. Lett. **76**, 163 (1980); P. C. Hariharan and J. A. Pople, Theor. Chim. Acta **28**, 213 (1973).

[21] A. J. H. Wachters, J. Chem. Phys. **52**, 1033 (1970); P. J. Hay, *ibid.* **66**, 4377 (1977): K. Raghavachari and G. W. Trucks, *ibid.* **91**, 1062 (1989).

[22] C. Peng and H. B. Schlegel, J. Comput. Chem. **17**, 49 (1996).

[23] M. W. Wong, Chem. Phys. Lett. **256**, 391 (1996).

[24] F. Hǿjland, H. Toftlund, and S. Yde-Anderson, Acta Chem. Scand. A **37**, 251 (1983).

[25] R. Rüffer and A. I. Chumakov, Hyperfine Interact. **97/98**, 589 (1996).

[26] T. Ishikawa, Y. Yoda, K. Izumi, C. K. Suzuki, X. W. Zhang, M. Ando, and S. Kikuta, Rev. Sci. Instrum. **63**, 1015 (1992); T. Toellner, T. Mooney, S. Shastri, and E. E. Alp, Proc. SPIE **1740**, 218 (1992).

[27] A. Q. R. Baron, Nucl. Instrum. Methods Phys. Res. A **352**, 665 (1995).

[28] H. Grünsteudel, Ph.D. thesis, University of Lübeck, 1998.
[29] R. K. Khanna, C. W. Brown, and L. H. Jones, Inorg. Chem. **8**, 2195 (1969); G. Paliani, A. Poletti, and A. Santucci, J. Mol. Struct. **8**, 63 (1971); L. Tosi, Spectrochim. Acta A **29**, 353 (1973).
[30] J. B. Bates and R. K. Khanna, Inorg. Chem. **9**, 1376 (1970); O. Zakharieva, Th. Woike, and S. Haussühl, Spectrochim. Acta A **51**, 447 (1995).
[31] M. R. Pressprich, M. A. White, Y. Vekhter, and P. Coppens, J. Am. Chem. Soc. **116**, 5233 (1994).
[32] D. A. Estrin, L. M. Baraldo, L. D. Slep, B. C. Barja, J. A. Olabe, L. Paglieri, and G. Corongiu, Inorg. Chem. **35**, 3897 (1996).